A&A 446, 223–235 (2006)
DOI: 10.1051/0004-6361:20053150

Astronomy & Astrophysics

Asteroseismological constraints on the structure of the ZZ Ceti star HL Tau 76

D. Pech, G. Vauclair, and N. Dolez

Université Paul Sabatier, Observatoire Midi-Pyrénées, CNRS/UMR5572, 14 Av. E. Belin, 31400 Toulouse, France
e-mail: gerardv@ast.obs-mip.fr

Received 29 March 2005 / Accepted 23 August 2005

ABSTRACT

This paper reports the results derived from an asteroseismological study of the cool ZZ Ceti star HL Tau 76. A grid of models has been computed in a parameter space covering the range of log g and $T_{\rm eff}$, formerly determined by spectroscopy, and a large range of hydrogen mass fraction. The adiabatic non-radial oscillations for all the models have been computed for the modes of degrees $\ell = 1$ and $\ell = 2$. An algorithm based on a χ^2 test was applied to evaluate the quality of the fit between observed and theoretical periods. This method resulted in selecting a best fitting model for which the average relative matching of the periods is 0.7%. Then, a detailed comparison between the observed and the computed periods for the $\ell = 1$ and $\ell = 2$ modes of the best fitting model was achieved in order to identify as many observed modes as possible. To perform this identification we used the calculated periods for which we applied the rotational splitting as deduced from the observations. Through this process we identify the 36 independent modes observed in HL Tau 76. The best fitting model for HL Tau 76 is well constrained due to the large number of oscillations detected in this ZZ Ceti star. The main stellar parameters of HL Tau 76 derived from this analysis are: the total mass $M_\star = 0.575 \pm 0.005\, M_\odot$, the hydrogen mass fraction $q_{\rm H}$, estimated as thick as $2.35 \pm 0.10 \times 10^{-4}$. The helium mass fraction consistent with $q_{\rm H}$ must be $q_{\rm He} = 1 \times 10^{-2}$. The method is not sensitive to $T_{\rm eff}$ variations in the narrow domain of temperature derived from spectroscopy for HL Tau 76. The best adjustment is found however for $T_{\rm eff} = 11\,375$ K. The other derived stellar parameters are the luminosity ($L/L_\odot = 0.00389$) and the radius ($R/R_\odot = 0.0162$). We note some trends in the fit of the observed periods with the computed ones which suggest that the rotational splitting could be non-uniform and that the large amplitude modes might contain information on the convection-driven excitation mechanism.

Key words. stars: fundamental parameters – stars: white dwarfs – stars: oscillations – stars: individual: ZZ Ceti, HL Tau 76

1. Introduction

Asteroseismology is a powerful tool to infer precisely the internal structure of variable stars. By comparing their observed periods of oscillation with the periods predicted by the theory of non-radial pulsations, it is possible to derive the structure of the model or of the set of models which fits best the observations. This direct method has been successfully applied to the pulsating pre-white dwarfs of PG 1159 type (see for instance Winget et al. 1991; Vauclair et al. 2002) and to the pulsating DB white dwarfs (Winget et al. 1994). In the case of the pulsating DA white dwarfs (the ZZ Ceti stars), the application of the method has been less successful, mainly because of the smaller number of oscillation modes observed in those stars, compared to the rich spectrum observed in the hotter classes of pulsating white dwarfs. The models are consequently not so well constrained for the ZZ Ceti stars and the solution is generally not unique. The results from the asteroseismological analysis of 9 ZZ Ceti stars observed with the Whole Earth Telescope (WET; Nather et al. 1990) are discussed in Kepler et al. (1995) for G 226-29, Bradley (2001) for L 19-2, Bradley (1998) and Mukadam et al. (2003) for R 548, Bergeron et al. (1993) and Bradley (2001) for GD 165, Kleinmann et al. (1998) for G 29-38, Bradley (1998) for G 117-B15A, Pfeiffer et al. (1996) for GD 154, Kanaan et al. (2005), Metcalfe et al. (2004) and Fontaine & Brassard (2004) for BPM 37093 and Castanheira et al. (2004) for G 185-32.

However, the ZZ Ceti white dwarfs constitute the most numerous class of variable white dwarfs. About 70 ZZ Ceti stars are known after the recent discovery of 35 new ones from the Sloan Digital Sky Survey (SDSS) first release catalog (Mukadam et al. 2004a). Knowing the internal structure of DA white dwarfs is important in many respects and justifies the continuous effort to derive it from asteroseismology. The ZZ Ceti instability strip takes a trapezoidal form in the H-R diagram because of the dependence of its blue and red boundaries on the stellar mass. However, the width and the limits of the instability strip differ in the two samples of Bergeron et al. (2004) and of Mukadam et al. (2004b). More importantly, while Bergeron et al. (2004) find a *pure* instability strip, with no non-variable DA stars within the instability strip in their sample, Mukadam et al. (2004b) reach a different conclusion from the analysis of the SDSS sample which contains non-variable stars inside the instability strip. Whether this results from a genuine cohabitation of pulsators and non-pulsators within the instability strip or from larger uncertainties in the atmospheric

parameters derived from the lower S/N SDSS spectra needs to be further investigated. However, the brightest of the non-pulsators that Mukadam et al. (2004b) find to lie within their instability strip is a $g = 17.1$ mag star. The spectrum used to derive its atmospheric parameters has a S/N ratio of 35 (Kleinman et al. 2004). The S/N ratio for the fainter DA white dwarfs is of course lower. This makes the uncertainty on the location of the stars in the region of the instability strip larger than in the brighter Bergeron et al. (2004) sample for which the derived atmospheric parameters rely on $S/N \geq 80$ spectra. This may explain why both pulsators and non-pulsators seem to overlap in the SDSS sample. If the instability strip is a *pure* one, then it is an indication that the structure of the ZZ Ceti white dwarfs derived from asteroseismology could be considered as representative of the structure of the DA white dwarfs as a whole group.

The DA white dwarfs represent 80% of the total white dwarf population (Fleming et al. 1986) and 97% of the stars in the Galaxy are predicted to end their evolution as white dwarfs. Those stars are therefore of major interest: infering accurately their internal structure is of prime importance to better understand the process of stellar evolution. Their cooling sequence can be used to determine the distances to galactic globular clusters (Salaris et al. 2001). Moreover, as they are the oldest stars in the Galaxy, they can be used to determine the age of the stellar population to which they belong. Consequently, considerable efforts have been made to improve our knowledge of the white dwarfs so that it can be used for cosmochronology (Winget et al. 1987; Fontaine et al. 2001). The method consists of comparing the observed white dwarf luminosity function with the one built from computed cooling sequences. The accuracy of this method depends on the precision with which one knows the structure of the white dwarf models used to build the cooling sequences. The main uncertainties in those models are: 1) the total mass and the precise chemical composition of the degenerate C/O core (i.e. the C/O ratio and its distribution as function of the radius); this is what determines the total thermal energy available for the cooling; 2) the mass fraction of the outer layers (He and H); this is what determines the rate at which the thermal energy stored in the core is transported to the stellar surface and radiated outward; in this respect, the hydrogen mass fraction is the most important quantity since the hydrogen opacity overwhelms that of He; a wide hydrogen mass fraction distribution would translate into a similarly wide age distribution at a given luminosity and would considerably weaken the usefulness of the white dwarf cooling sequence for cosmochronology; 3) the way the crystallization occurs in the C/O core.

Determining the hydrogen mass fraction in DA white dwarfs is also a clue to the chemical evolution of the white dwarfs along their cooling sequence. It determines if, and at what effective temperature (or luminosity), the convection zone in the hydrogen envelope reaches the H/He transition zone and mixes with the underlying helium convection zone, changing the spectral type from DA to DB or DC. This long-debated question on whether DA white dwarfs have a "thin" or a "thick" hydrogen envelope is reviewed by Fontaine & Wesemael (1997).

The asteroseismology of the ZZ Ceti white dwarfs can potentially constrain some of these quantities. The total mass and the hydrogen mass fraction have a strong impact on the g-mode pulsation spectrum. One can derive these quantities accurately enough. The average chemical composition of the degenerate C/O core could be derived in principle from a measurement of $\dot{P}$, the rate of change of the pulsation periods. However, this measurement requires that there exist pulsation modes stable enough in period and amplitude so that we may be sure that they are not involved in some complex physical processes such as mode coupling, mode resonance, coupling with convection, and so on. In addition, the $\dot{P}$ of a given mode would be a measure of the rate of cooling only if this mode propagates deep enough to "feel" part of the degenerate core (i.e. the mode is not trapped in a shallow hydrogen envelope). Finding such suitable pulsation modes for a $\dot{P}$ measurement should be more likely in the hot ZZ Ceti pulsators since the interaction of the convection with the pulsations, which increases as the white dwarfs cool within the ZZ Ceti instability strip, is still negligeable close to the blue edge. Even in those favourable circumstances, a few decades are required to obtain a significant $\dot{P}$ measurement (see for instance Kepler et al. 2000). Montgomery et al. (2003) have shown that the signature of the chemical transition regions on the period distribution, the mode trapping, may not be unambiguously interpreted in some circumstances. They found that the bumps in the Brunt-Väisälä frequency due to these transitions induce a core/envelope symmetry in the mode trapping. A chemical transition within the core, between its C/O central region and its progressively richer C external region, may have a similar mode trapping signature to the chemical transition zones in the envelope. These could be the He/C–O–He and C–O–He/C–O transitions in the DB white dwarf pulsators or the H–He and He/C–O transition zones in the DA pulsators. When the chemical transition zones are computed through a time-dependent diffusion scheme, as for instance in Córsico et al. (2005) or Brassard & Fontaine (2005), the outer transition zones may become so smooth that the structure inside the core dominates the mode trapping. However, in the case of the DA pulsators, Montgomery et al. (2003) showed that the H–He transition zone has no core counterpart as long as the hydrogen mass fraction exceeds $q_{\rm H} = (1 - M_{\rm H}/M_*) = 10^{-6}$. We will show in the next sections that it is the case for HL Tau 76.

Thus, asteroseismology is a potentially powerful tool to determine the fundamental parameters of the ZZ Ceti stars and more specifically their total masses and hydrogen mass fraction, two of the main uncertain parameters entering the modeling of white dwarf stars. In this respect, the ZZ Ceti HL Tau 76 is one of the most promising cases since it exhibits a rich oscillation spectrum.

HL Tau 76 was the first discovered ZZ Ceti star (Landolt 1968) and has been studied repeatedly, in particular during the Whole Earth Telescope multisite fast photometry campaigns XCOV13 and XCOV18. Much observational data are thus available as presented in detail by Dolez et al. (2006). The power spectrum is complex and the oscillations are gathered within very narrow frequency bands separated by large gaps. This makes difficult any direct observational determination of its *period spacing*, ΔP. Furthermore, the lack of a large enough

number of consecutive modes does not allow us to deduce the ΔP vs. P diagram, which would contain a potential signature of mode trapping. Dolez et al. (2006) made a preliminary asteroseismological analysis based on the assumption of a period distribution following the asymptotic regime. They showed that most of the observed periods were consistent with $\ell = 1$ and $\ell = 2$ expected periods and suggested an identification of those modes. Deriving the fundamental parameters of HL Tau 76, such as the total mass and the hydrogen mass fraction, implies calculating the g-mode oscillation spectra of realistic models and searching for the model that fits the observations with the best possible accuracy. This is what is developed in this paper. Section 2 briefly presents the observational data available for HL Tau 76. Section 3 introduces the modeling code used and discusses the strategy applied to isolate the best fitting candidate from our full grid of models. Section 4 describes the best fitting candidate and lists the periods of its $\ell = 1$ and $\ell = 2$ modes. Taking advantage of our knowledge of the rotational splitting, taken from the study of Dolez et al. (2006), we propose an identification for all the observed modes. Section 5 summarizes our results.

2. Observational background

The data relevant to HL Tau 76 observations are presented exhaustively in Dolez et al. (2006, DVK). We use the full set of the observed periods in this ZZ Ceti star, having removed the linear combinations of genuine modes. The complete list of these periods is given in Table 1 from the data coming from the WET campaigns XCOV13, XCOV18 and from earlier archival observations.

DVK find 43 periods which they identify as independent pulsation modes of degree $\ell = 1$ and $\ell = 2$ split by rotation. With such a number of modes, HL Tau 76 shows the currently richest oscillation spectrum among the ZZ Ceti stars. These periods cover a wide range, between 380 s and 1390 s. However their distribution reveals a striking peculiarity: many modes occupy very tight zones in frequency while large domains remain empty. This characteristic greatly complicates the analysis of this spectrum and makes the use of theory and modeling compulsory to deduce the structural properties of this ZZ Ceti star by asteroseismology. The rich oscillation spectrum should strongly constrain the internal structure of HL Tau 76 as shown in the next sections. See DVK for details regarding HL Tau 76 observational material and data reduction.

Table 1. Period (s) list of HL Tau 76 after Dolez et al.

XCOV18	XCOV13	Archives
1390.8		
	1347.9	1353.7
		1308.7
1070.8		
1067.5		
1065.0	1065.0	
1061.8		
1060.2		
979.2		
976.4		
974.4		
971.6		
933.2	932.5	
930.6		
799.1		
798.3		
796.4	796.5	
794.1		
792.7		
	781.0	
		748.5
738.7		
		689.3
664.2		665.0
663.6		
662.8		
662.3		
661.9		
661.4		
660.1		
659.5		
	657.4	
		628.0
598.6		
597.1	597.0	
596.8		
542.4		
541.8		
540.9	541.0	
494.2	494.2	495.0
493.2		
	449.8	
394.3		
382.5	382.5	

3. Modeling strategy

We calculate the non-radial g-modes in a grid of static models to compare their periods with those derived from observations and then to search for the best fitting solution. The code computes complete static models from the center to the surface through a shooting method. The differential equations are integrated outward from boundary conditions at the center, and inward from boundary conditions at the surface (indeed at optical depth $\tau = 2/3$). The integration algorithm uses a self-adapting Runge-Kutta routine to optimize the model layer depth. The number of mesh points is increased within the H/He and He/C transition zones to obtain an accurate description of these zones. The models typically have ≈700 layers of which ≈490 describe the hydrogen outer layer and the H/He transition zone, 40 the He layer and 170 the He/C transition zone and the core. This number of layers is sufficient for the required accuracy of the Brunt-Väisälä frequency of the model, i.e. the required accuracy of the g-mode frequencies. The convergence between the outward and inward integrations is obtained through a Newton-Raphson iterative method. The atmospheric structure is derived by fitting a T-τ relation from Koester's atmosphere models of $T_{\rm eff}$ and $\log g$ suitable for the HL Tau 76 atmospheric parameters. The OPAL Rosseland mean opacities (Iglesias & Rogers 1996) and EOS are used in the H and He

outer layers, with the appropriate interpolation within the transition zone. They are completed in the deeper layers by the electronic conductivity as tabulated in Itoh et al. (1983, 1984) and Mitake et al. (1984). Our models have a pure carbon core. Stellar evolution calculations predict that real white dwarf stars must have a C–O core whose composition and relative distribution depend on the previous stages of evolution. But as we compute static models, and not an evolutionary sequence, this simplification does not affect our models much since the equilibrium pressure is provided by the degenerate electrons through the mean molecular weight per free electron, μ_e, which is the same for C and O. In addition, Montgomery et al. (2003) have shown that a structure in the C/O profile within the core cannot mimic the signature of a H/He transition for a hydrogen mass fraction larger than $\approx 10^{-6}$. It will be shown below that the period distribution in HL Tau 76 requires a larger hydrogen mass fraction. As a consequence, any mode trapping found in the period distribution could not lead to an ambiguous identification.

In the carbon core, the EOS is taken from Fontaine et al. (1977). The convection is described by the mixing length theory in its ML2, $\alpha = 0.6$ version according to Bergeron et al. (1995).

The H/He and He/C transition zones are described in the element diffusion equilibrium approximation, as in Tassoul et al. (1990). This description relies on the trace element approximation. More realistic description of the chemical transition zones induced by diffusion, which do not use this approximation, have been incorported in recent works (Córsico et al. 2002; Metcalfe et al. 2003; Brassard & Fontaine 2005). Córsico et al. (2001, 2002) have computed fully evolutionary DA white dwarf models taking into account time dependent element diffusion. They found that the H/He transition zone in those models is smoother than in models computed within the equilibrium diffusion approximation. As a consequence, the mode trapping induced by the transition zone is weaker. However, since HL Tau 76 (with $T_{\rm eff} = 11\,450$ K) is cooler than their template model (12 000 K) of similar total mass, and therefore accordingly older, the H/He transition zone in HL Tau 76 must be closer to the equilibrium diffusion than in the hotter model of Córsico et al. In addition, it will be shown hereafter that the best fitting model for HL Tau 76 has a more massive hydrogen outer layer than the Córsico et al. template model. As a result, the effect of mode trapping decreases to the point where the differences in the structure of the H/He transition zone induced by the different prescriptions used to compute this zone have a negligeable effect on the periods, or at least one comparable to the other uncertainties entering the model computation. Thus, the description of the transition zone is accurate enough for this study. The Brunt-Väisälä frequency, N^2, is computed in the models according to the expression (Brassard et al. 1991):

$N^2 = g^2\varrho/P \times \chi_T/\chi_\varrho(\nabla_{\rm ad} - \nabla + B)$ with:

$B = -1/\chi_T\ (\partial \ln P/\partial \ln Y)_{\varrho,T}\ {\rm d}\ln Y/{\rm d}\ln P$

where Y is the relative helium abundance and with the thermodynamic quantities:

$\chi_{\rm T} = (\partial \ln P/\partial \ln T)_{\varrho,Xi}$ and $\chi_\varrho = (\partial \ln P/\partial \ln \varrho)_{T,Xi}$.

The B term is non-zero only in the chemical transition zones. As the $(\partial \ln P/\partial \ln Y)_{\varrho,T}$ term tends to zero with increasing degeneracy , the influence of the B term decreases as the H and He mass fraction increases since the transition zones occur in a region of larger degeneracy. That is why the mode trapping decreases with increasing H and He mass fraction. The non-radial g-modes are computed in the adiabatic approximation for each model. We only consider the $\ell = 1$ and $\ell = 2$ modes since modes of higher ℓ degrees are unlikely to be observed. DVK find that all the periods observed in HL Tau 76 are consistent with the period distribution expected in the asymptotic regime for $\ell = 1$ and $\ell = 2$ modes. The pulsation periods computed in the adiabatic approximation are accurate enough for a comparison with the observed periods. The computation of the kinetic energy associated with each pulsation mode allows us to identify the potential trapped modes in the pulsation spectrum of a model when the thickness of the hydrogen and the helium layers favours the *mode trapping* phenomenon. As it is well known, the trapped modes present a lower kinetic energy than normal modes and in a plot of the kinetic energy as a function of period, the trapped modes appear as local minima. Under the condition that a sufficiently large number of consecutive order modes (k) of a given degree (ℓ) are observed, the period difference between consecutive modes (ΔP), when plotted as a function of the period (P), provides a ΔP vs. P diagram which, together with the minima in the kinetic energy plot, is useful to deduce the *trapping cycle* of the star. The average *period spacing* ΔP and the ΔP vs. P diagram with the *mode trapping* then strongly constrain the main features of the stellar structure: its hydrogen (and possibly its He) mass fractions and its total mass. In the case of HL Tau 76, there are not enough consecutive order modes in the available observational data. It is not possible to make such a ΔP vs. P diagram. We have to rely on the direct comparison of the periods calculated in the grid of models with the observed ones. The computed kinetic energy may then be used to identify the nature, trapped or untrapped, of the modes observed in HL Tau 76.

The first step consists of building a grid of white dwarf models. The structure of these models depends mostly on 7 parameters:

- the total stellar mass $M_\star$;
- the hydrogen layer mass fraction, $q({\rm H}) = M({\rm H})/M_\star$;
- the effective temperature $T_{\rm eff}$;
- the helium layer mass fraction, $q({\rm He}) = M({\rm He})/M_\star$;
- the core composition;
- the rotation rate of the star and the possible differential rotation inside the star;
- the version of the mixing length theory (MLT).

Only the first 3 ones have been varied in our study. The helium mass fraction is a dependent parameter whose value is constrained by the mass of the hydrogen envelope, according to the arguments developed later in this section. The stellar core is considered as a pure carbon degenerate core as justified above; the effect of stellar rotation, differential or not, on the stellar structure is ignored. But the rotational splitting induced by the rotation in the power spectrum of HL Tau 76 is taken into account in our identification procedure of the observed modes;

as for the mixing length theory, the ML2 version with $\alpha = 0.6$ has been adopted, according to the analysis of Bergeron et al. (1995).

Bergeron et al. (1995) determined the atmospheric parameters of HL Tau 76 from spectroscopy: $\log g = 7.89$ (±0.05) and $T_{\rm eff} = 11\,450$ K (±350 K). They note that their adopted uncertainties on $T_{\rm eff}$ are conservative overestimates. More recently Bergeron et al. (2004) revised the $T_{\rm eff}$ uncertainties in their sample to ±200 K. The surface gravity translates into a total mass $M_\star = 0.55\ M_\odot$ (±0.03 $M_\odot$) for a thick hydrogen model (q(H) = 10^{-4}) and q(He) = 10^{-2} according to the models of Wood (1995). These values for the total mass and $T_{\rm eff}$ are taken as starting points for the computation of our grid of models. The uncertainty on the spectroscopically determined mass and $T_{\rm eff}$ confines those parameters within a narrow range. The main parameter left which strongly affects the periods of the g-modes is q(H). Therefore, the size of the space parameters to be explored for modeling HL Tau 76 is reasonably small. The computation of the grid of models does not require the use of a time consuming method based on a genetic algorithm. The helium mass fraction was initially fixed at $\log q$(He) = −2, which is the commonly assumed value for this parameter. The determination of the helium mass fraction from asteroseismology remains a difficult exercise since the pulsation modes are rather insensitive to this parameter.

For the q(H) values, we first chose a rough cut with wide grid meshes, which was later refined according to the preliminary results.

The comparison between the computed periods and the observed modes is based on a χ^2 test algorithm. For each model of the grid and each observed period, the algorithm searches for the closest period within the $\ell = 1$ and the $\ell = 2$ periods from the model. Then it computes the square of the difference between the two periods. It proceeds following this for all the observed periods while adding the squares and consequently obtains a sum of least squares (χ^2). The lower the χ^2, the better the agreement between computed and observed periods.

We only considered the $\ell = 1$ and $\ell = 2$ modes since modes with higher ℓ degrees are very unlikely to be actually observed. When several frequencies are observed in the same narrow range of the power spectrum of HL Tau 76, we keep only the average value of these frequencies in order not to bias the resulting χ^2 by favouring these groups of modes. This is justified by the fact that such close frequencies are supposed to be various components of a multiplet generated by a single mode split by rotation. This unproved assertion is however validated a posteriori in Sect. 4. In the list of the observed periods, we profit from the preliminary classification between the possible $\ell = 1$ and $\ell = 2$ modes as presented by DVK. Nonetheless, their mode identification (Table 6) is based on the assumption that the observed period distribution closely follows the expected asymptotic regime. From the present study, we can now compare the observed periods with the periods calculated in realistic models, which do not need to follow closely this asymptotic regime period distribution. For this reason, we rely here on their Tables 5-1 and Table 5-2 which still reflects the possibility of some observed pulsations being either $\ell = 1$ or $\ell = 2$ modes. Furthermore, the distinction between the presumably $\ell = 1$ or $\ell = 2$ modes has to be included in our process: we must compare computed and (supposed) observed modes relevant to the same ℓ degree. Otherwise, the algorithm could associate computed $\ell = 1$ modes with observed $\ell = 2$ modes and vice versa. Such a mismatch would spoil the validity of the results derived from the algorithm. Nonetheless, when DVK mention that a given mode may be a $\ell = 1$ as well as a $\ell = 2$ mode or when they cannot assign a value for the ℓ degree, this one is included in the two lists of observed modes classified according to their supposed ℓ degree.

In the first grid of models we let two parameters vary: the hydrogen mass fraction takes the values $\log q$(H) = −4, –6, –8 and –10 and the $T_{\rm eff}$ takes the successive values 11 350 K, 11 450 K and 11 550 K. This range in $T_{\rm eff}$ takes into account the uncertainty as given by Bergeron et al. (2004). The stellar mass is kept fixed at 0.55 $M_\odot$.

The algorithm failed to discriminate the effective temperature. This is not surprising since, in this narrow range of $T_{\rm eff}$, the models do not change significantly, all other parameters being kept fixed. By contrast, it systematically selected the models with the highest hydrogen mass fraction with $\log q$(H) ≥ −6 as the best candidates. We consequently refined the grid by computing and analysing extra models with $\log q$(H) = −5, –4.3, –3.3 and –3. For this second grid of models, we kept the same mesh in $T_{\rm eff}$. The models with $\log q$(H) = −3 are probably not realistic since stellar evolution does not predict such a large amount of remaining hydrogen at the white dwarf stage. But they were nonetheless quite useful to identify the minimum χ^2 by showing that it increases again sharply, once the optimal value of q(H) is exceeded. A full set of 24 models has thus been analysed with the algorithm. For each value of $q(H)$, the 3 χ^2 relevant to the 3 different $T_{\rm eff}$ were averaged for the $\ell = 1$ and the $\ell = 2$ modes respectively. These results are shown in Figs. 1 and 2.

Both Figs. 1 and 2 make clear that the lowest χ^2 is reached for models with q(H) = 1 up to 5×10^{-4}. In order to get the statistically most probable value for q(H), a weighted mean was calculated over the 8 best models (excluding models with q(H) = 10^{-3} since they are rather unrealistic), the weighting coefficients being inversely proportional to the χ^2 pertaining to the considered model. The weighted means derived for the $\ell = 1$ and the $\ell = 2$ modes are in perfect agreement and both lead to a value of q(H) = 2.35×10^{-4}. The hydrogen mass fraction in HL Tau 76 has thus been constrained.

The large value deduced for q(H) involves a tight constraint on q(He) due to two theoretical considerations. The first one, which is also the strongest, sets an upper limit near q(He) = 10^{-2} for the helium mass fraction so as to prevent the bottom of this layer from being hot enough for fusion. The second condition imposes that the helium envelope must be roughly 50 to 100 times thicker than the external hydrogen layer to avoid overlap between both the H/He and the He/C transition zones. Indeed, if these two zones overlaped, carbon could diffuse and reach the stellar surface, and yet carbon lines are not observed in the ZZ Ceti spectra. To have these two conditions simultaneously satisfied, there is only one possible value suitable for

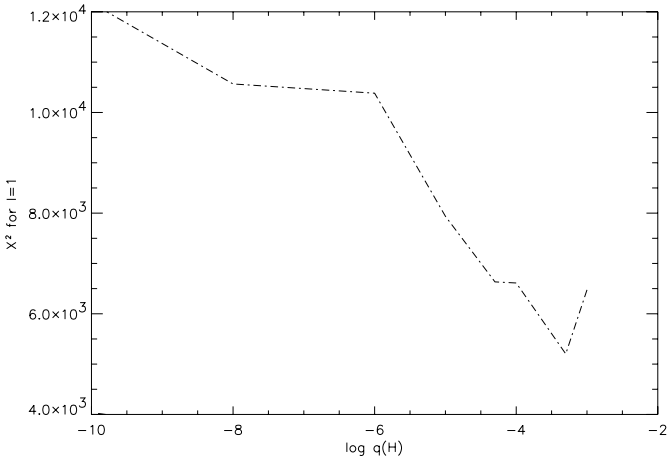

Fig. 1. χ^2 vs. $\log q$(H) for $\ell = 1$ modes with $M_\star = 0.55\,M_\odot$.

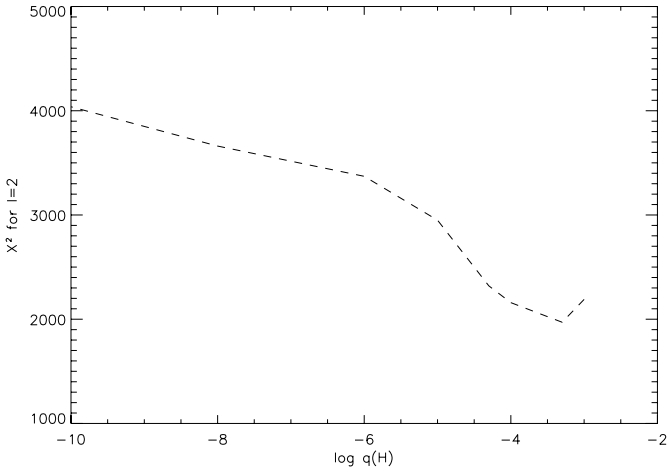

Fig. 2. Same as Fig. 1 but for $\ell = 2$ modes.

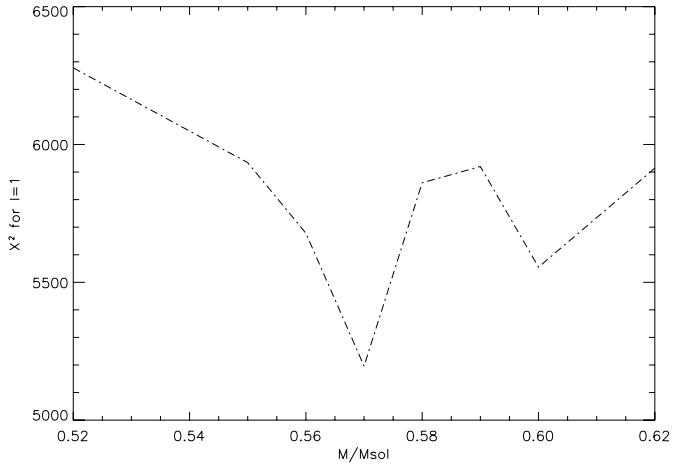

Fig. 3. χ^2 vs. $M_\star$ for $\ell = 1$ modes.

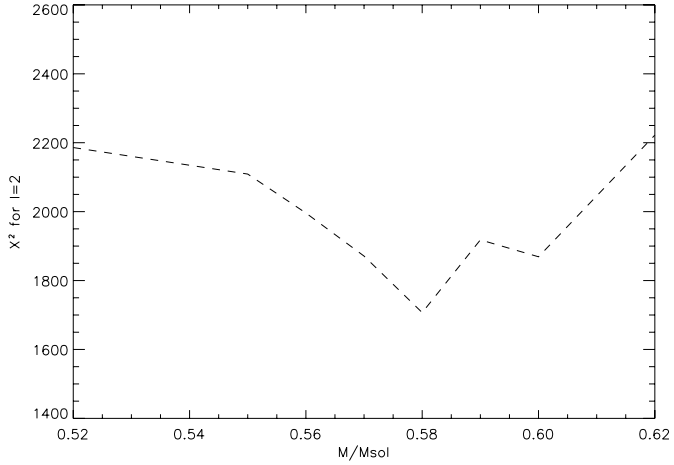

Fig. 4. χ^2 vs. $M_\star$ for $\ell = 2$ modes.

the helium mass fraction: q(He) $= 10^{-2}$, which is moreover the value generally adopted for modeling DA white dwarfs and most of the ZZ Ceti stars.

The next step is to evaluate the whole stellar mass and the effective temperature of HL Tau 76 to complete the determination of the free stellar parameters. After Bergeron et al. (1995), the spectroscopic determination of the surface gravity, $\log g = 7.89$ (±0.05), leads to a mass of 0.55 $M_\odot$ (±0.03 $M_\odot$). The allowable range of mass for HL Tau 76 spreads thus between 0.52 $M_\odot$ and 0.58 $M_\odot$. However, we slightly exceeded those limits to clearly identify the lowest χ^2. All the models in this series used to determine the mass of HL Tau 76 have the same q(H) $= 2.35 \times 10^{-4}$ and q(He) $= 10^{-2}$. The $T_{\rm eff}$ takes again the three previously assigned values: 11 350 K, 11 450 K and 11 550 K.

For the $M_\star$ values, we selected: 0.52 $M_\odot$, 0.55 $M_\odot$ and 0.58 $M_\odot$ in a first run. According to these first models, the algorithm indicates that the total mass of HL Tau 76 appears to lie near the upper limit. Thus, we completed our grid with models of 0.56, 0.57, 0.59, 0.60 and 0.62 $M_\odot$. The two largest values for $M_\star$ are by far greater than the maximal mass allowed by spectroscopic determination. However, we kept these models because they are necessary to precisely confine the best fitting mass in the χ^2 vs. $M_\star$ plane as illustrated in Figs. 3 and 4.

For the $\ell = 1$ modes (Fig. 3), the χ^2 algorithm favours the model with 0.57 $M_\odot$ whereas the 0.58 $M_\odot$ model is preferred in the case of the $\ell = 2$ modes (Fig. 4). These two results are coherent and suggest $M_\star$= 0.575 $M_\odot$ (±0.005 $M_\odot$) as the best total mass for HL Tau 76. This mass determination agrees with the upper limit allowed by spectroscopy. Also, the χ^2 tests reveal a secondary minimum for 0.60 $M_\odot$ for both the $\ell = 1$ and $\ell = 2$ modes. This value however falls outside the range allowed by spectroscopy and is less pertinent than the 0.57–0.58 $M_\odot$ minima in terms of χ^2. It thus can be rejected confidently and we keep 0.575 $M_\odot$ (±0.005 $M_\odot$) as the unambiguous mass of HL Tau 76.

Now that the mass of HL Tau 76 is accurately determined, it is necessary to check a posteriori the validity of the hydrogen mass fraction determination since it was obtained in the first step with models whose mass was fixed at 0.55 $M_\odot$. Another grid of models has been computed and analysed, with a total mass of 0.575 $M_\odot$ instead of 0.55 $M_\odot$. In this grid, we did not consider models with $\log q$(H) ≤ -6 and built additional models with $\log q$(H) $= -3.4$, -3.5 and -3.6. The χ^2 test applied to this grid selected the model with $\log q$(H) $= -3.6$ as the

best one, as well as for the $\ell = 1$ as for the $\ell = 2$ modes. It confirmed the former hydrogen mass fraction determination: $q(\mathrm{H}) = 2.35 \times 10^{-4}\, M_\star$. To test whether the effective temperature can be constrained better, we explored models with an enlarged $T_{\rm eff}$ distribution. From spectroscopic data, Bergeron et al. (1995) originally suggested that HL Tau 76 has an effective temperature ranging from 11100 K to 11 800 K and centered on 11 450 K. This range comes from a conservative overestimate of the uncertainty on $T_{\rm eff}$ as discussed by Bergeron et al. (1995). We used this full range of $T_{\rm eff}$ for this test. We built two parallel grids sharing the same hydrogen mass fraction, $q(\mathrm{H}) = 2.35 \times 10^{-4}$, and the same helium mass fraction, $q(\mathrm{He}) = 10^{-2}$. The models have a total mass of 0.575 $M_\odot$ in the first series and 0.565 $M_\odot$ in the second one. The second set of models is used to check that the sensitivity of the algorithm on the variation of $T_{\rm eff}$ does not behave differently for slightly different masses. The models are computed with an average difference of 30 K between two consecutive models in the first grid and 60 K in the second one. The resulting χ^2 did not select any particular best value of the effective temperature. In the HL Tau 76 range of $T_{\rm eff}$, the period distribution is not sensitive enough to slight variations of $T_{\rm eff}$ for this parameter to be precisely determined from a global χ^2 test. We examined case by case each model in the grid with $M_\star = 0.575\, M_\odot$ to compare their respective computed periods with the HL Tau 76 real spectrum in order to extract the best fitting candidate. The differences between model spectra for the same ℓ degree were weak, which illustrates once again that the effective temperature does not influence the pulsation periods. Nonetheless, a careful analysis of the overall $\ell = 1$ and $\ell = 2$ spectra defined the model with 11 375 K as the best possible one.

4. Identifying HL Tau 76 pulsation modes

4.1. The best model

Now that the determination of HL Tau 76 stellar parameters is completed, it is possible to study the properties of our best fitting model. The modeling strategy used to place constraints on the HL Tau 76 internal structure sets 3 free stellar parameters and resulted in isolating a best candidate in our full grid of models. This best fitting model has a full mass $M_\star = 0.575\, M_\odot$, a hydrogen envelope as thick as $q(\mathrm{H}) = 2.35 \times 10^{-4}$, a helium layer mass $q(\mathrm{He}) = 10^{-2}$ and an effective temperature $T_{\rm eff} = 11\,375$ K. To estimate the uncertainty on the derived total mass and hydrogen mass fraction, we evaluate how much those quantities have to change to induce 10% increase of the χ^2 relatively to their minimum values. The inferred total mass uncertainty is 0.005 $M_\odot$ while the uncertainty on the hydrogen mass fraction is $10^{-5}\, M_*$. From these parameters, we induce the luminosity and the radius: $\log(L/L_\odot) = 0.00389$ and $R = 0.0162\, R_\odot$. These parameters of our best candidate are summarized in Table 2. We computed the $\ell = 1$ and $\ell = 2$ adiabatic modes for this best fitting model and then attempted to match the computed periods with the observed ones. While performing this task, we took the observed *rotational splitting* into account since the periods are computed for $m = 0$ modes whereas the observed modes may correspond to any m value between -ℓ and +ℓ. The results of our adiabatic calculations for the $\ell = 1$ and the $\ell = 2$ modes are given in Tables 3a and 3b. The comparison of these tables shows that a number of $\ell = 1$ and $\ell = 2$ modes have very close periods. Within the range of the observed periods, between ≈380 s and ≈1390 s, 20 $\ell = 1$ modes and 36 $\ell = 2$ modes are found. Among them, 10 modes overlap in period with a relative period difference smaller than 0.8%. It is consequently not surprising that the precise identification of the observed periods may remain ambiguous in these overlapping frequency domains. The rotational splitting is an additional complication.

Table 2. Best fitting model parameters.

Stellar mass	$M_\star = 0.575(\pm 0.005)\, M_\odot$
Effective temperature	$T_{\rm eff} = 11375(\pm 30)$ K
Hydrogen layer mass	$M(\mathrm{H}) = 2.35\ (\pm 0.10) \times 10^{-4}\, M_\star$
Helium layer mass	$M(\mathrm{He}) = 10^{-2}\, M_\star$
Luminosity	$(L/L_\odot) = 0.00389$
Stellar radius	$R = 0.0162\, R_\odot$

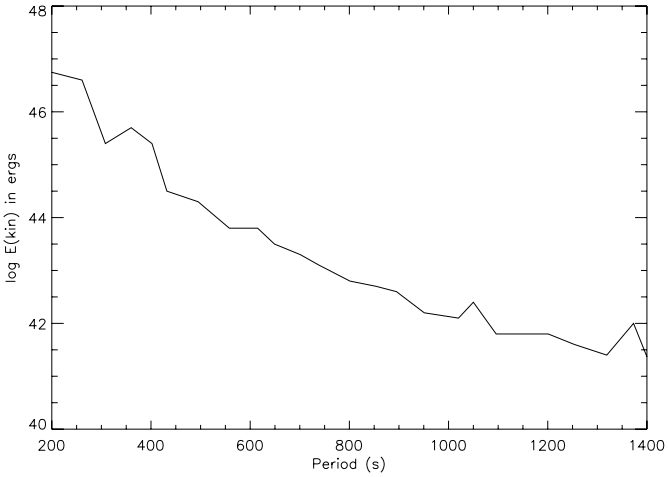

Fig. 5. $\log E_{\rm kin}$ vs. P for $\ell = 1$ modes for the best fitting model.

It is now well established that a thick hydrogen layer in a ZZ Ceti star is not favourable to *mode trapping* (see for instance Brassard et al. 1992). Since we find that the best fitting model for HL Tau 76 has a very thick hydrogen layer, its power spectrum will probably not show a signature of mode trapping. As a result, plotting the kinetic energy of its pulsation modes versus their respective period is not likely to show a minimum in the curve. This theoretical prediction is verified in Figs. 5 and 6 which display respectively the $\ell = 1$ and the $\ell = 2$ modes kinetic energy versus their period.

4.2. Predicted and observed spectra. Period identification

Selected models of HL Tau 76 can be tested by comparing their pulsation periods with the modes observed in the real star. The periods of the $\ell = 1$ and $\ell = 2$ modes for the best fitting model are listed in Tables 3a and 3b. These lists are restricted to a domain of periods covering the observed range, extended towards the shorter periods down to the order $k = 1$. From Table 3a,

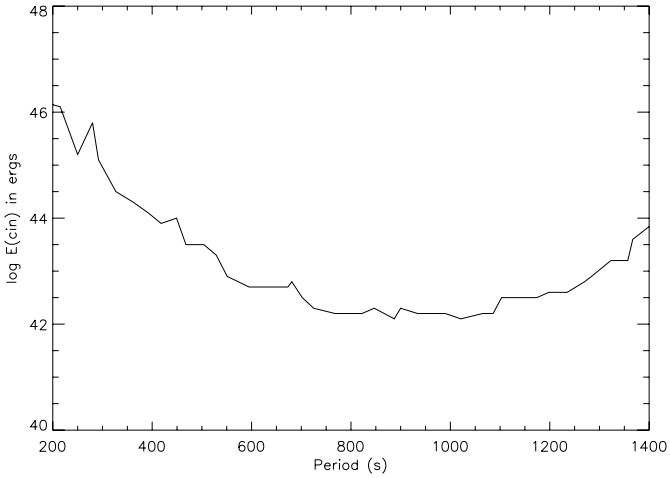

Fig. 6. $\log E_{\rm kin}$ vs. P for $\ell = 2$ modes for the best fitting model.

Table 3a. $\ell = 1$ modes periods for the best fitting model.

k	Period (s)	k	Period (s)
1	135.4	14	853.6
2	265.2	15	900.0
3	305.4	16	951.7
4	361.1	17	1015.7
5	401.2	18	1059.2
6	431.5	19	1094.7
7	499.0	20	1152.5
8	557.0	21	1201.0
9	613.5	22	1256.8
10	651.8	23	1312.7
11	698.7	24	1376.7
12	742.5	25	1406.9
13	801.6	26	1455.1

the average period spacing for the $\ell = 1$ modes predicted in the best fitting model, ($\overline{\Delta P}_{\ell=1,th}$) is obtained. We evaluated $\overline{\Delta P}_{\ell=1,\rm th}$ between the mode $\ell = 1$, $k = 4$ (period 361.1 s) and the mode $\ell = 1$, $k = 25$ (period 1406.9 s). This range roughly fits the periods observed in HL Tau 76 and avoids the low order k modes which may significantly depart from the asymptotic regime. We find $\overline{\Delta P}_{\ell=1,\rm th} = 49.8$ s. This value can be compared with the average period spacing that DVK suggest for the supposed $\ell = 1$ modes observed in HL Tau 76 ($\overline{\Delta P}_{\ell=1,\rm obs} = 48.0$ s). The two values are in good agreement.

Similarly, from Table 3b, we obtain $\overline{\Delta P}_{\ell=2,\rm th}$, the average period spacing for the $\ell = 2$ modes for the best fitting model. We calculate $\overline{\Delta P}_{\ell=2,\rm th}$ between the mode $\ell = 2$, $k = 9$ (period 360.1 s) and the mode $\ell = 2$, $k = 45$ (period 1391.2 s), which corresponds also to high enough values of k for the asymptotic regime to be valid. We get $\overline{\Delta P}_{\ell=2,\rm th} = 28.6$ s. This value is also in good agreement with the value $\overline{\Delta P}_{\ell=2,\rm obs} = 27.7$ s. that DVK derived for the average period spacing of the $\ell = 2$ modes.

The satisfactory agreement between the observational and theoretical average period spacings, for both $\ell = 1$ and $\ell = 2$ modes, indicates that our selected candidate should be a good representation of HL Tau 76.

1. **Multiplets caused by the *rotational splitting***
   The closely spaced frequencies in the Fourier spectrum are usually due to *rotational splitting*. An ℓ mode is split into a $(2\ell + 1)$ multiplet. The frequency shift between the components of the multiplets is used to estimate the stellar rotation rate while the number of the components in a multiplet allows identification of the ℓ value. In HL Tau 76, the situation is made complex by the fact that some multiplets due to the rotationally split $\ell = 1$ and $\ell = 2$ modes overlap. However, we can use the periods computed in the best fitting model (which are for the $m = 0$ component for each ℓ and k mode) together with the value of the average rotational splitting as derived from the observations (DVK) to fit the observed periods. We assume here that the observed period distribution in HL Tau 76 may be reproduced by such $\ell = 1$ and $\ell = 2$ modes split by rotation. We do not consider the possible additional effect of a weak magnetic field on the frequency shift.
   The frequency of the rotationally split modes of degree ℓ and order k are related to the frequency of the $m = 0$ mode by: $\sigma_{k,\ell,m} = \sigma_{k,\ell} + m \times (1 - C_{k,\ell}) \times \Omega$ with $C_{k,\ell} = \frac{\int_0^R \rho r^2 [2a(r)b(r)+b(r)^2]{\rm d}r}{\int_0^R \rho r^2 [a(r)^2+\ell(\ell+1)b(r)^2]{\rm d}r}$ after Ledoux & Walraven (1958).
   In this last expression a stands for the radial elementary displacement and b for the tangential elementary displacement. When the radial order is high (case of the *asymptotic limit*), $C_{k,\ell} \sim 1/[\ell(\ell + 1)]$. With $\delta f = (1 - C_{k,\ell}) \times \Omega$, we derive within the asymptotic limit approximation: $\delta f_{\ell=1} = 0.6\ \delta f_{\ell=2}$. This last relation leads to a good estimate for $\delta f_{\ell=2}$ given $\delta f_{\ell=1}$ and *vice versa*. From the observed multiplets in the power spectrum of HL Tau 76, DVK found $\delta f_{\ell=1} = 2.54\,\mu$Hz and therefore $\delta f_{\ell=2} = 4.23\,\mu$Hz. These values were obtained from a small number of identified multiplets. Here, we will assume that these values are correct for the whole range of frequencies observed in HL Tau 76. We can then calculate the frequency for all the components of a multiplet corresponding to any $\ell = 1$ or $\ell = 2$, $m = 0$ mode computed by the program. Rigorously, the numerical expressions derived for $\delta f_{\ell=1}$ and for $\delta f_{\ell=2}$ from the asymptotic limit are valid only for high radial overtones. As discussed by DVK and as confirmed by the identification of the modes proposed hereafter, the modes observed in HL Tau 76 correspond to order $k \geq 4$ for the $\ell = 1$ modes and to $k \geq 10$ for the $\ell = 2$ modes. We trust that these values of k are large enough for the asymptotic regime to be valid in the case of HL Tau 76.
2. **Matching computed and observed modes**
   The identification for all the modes observed in HL Tau 76 is provided in Table 4. The first column lists the computed periods which best fit the observed ones, taking the rotational splitting effect into account. The next three columns give the proposed identification for the degree ℓ, the order k and the azimuthal number m. The fifth column lists the observed periods to be compared to the computed ones. The absolute difference between observed and computed periods, $|\overline{\delta P}|$, is given in the next column. When slightly different values of the observed periods are alloted to a same

Table 3b. $\ell = 2$ modes periods for the best fitting model.

k	Period (s)	k	Period (s)
1	78.2	24	798.7
2	154.4	25	825.1
3	177.2	26	846.2
4	214.3	27	877.9
5	246.5	28	905.3
6	276.7	29	929.9
7	292.8	30	960.2
8	323.8	31	991.8
9	360.1	32	1015.5
10	389.8	33	1052.0
11	417.4	34	1086.3
12	444.1	35	1105.1
13	468.5	36	1132.9
14	500.0	37	1167.1
15	527.2	38	1197.4
16	552.6	39	1220.9
17	589.1	40	1260.8
18	623.7	41	1288.6
19	648.2	42	1304.8
20	671.5	43	1342.9
21	697.0	44	1374.2
22	727.6	45	1391.2
23	759.1	46	1424.4

mode, as it happens in a few cases for periods derived from different data sets, we take the average value. The last column gives the relative differences between observed and computed periods. In some cases of ambiguous identifications between different ℓ values, we chose the solution that offered both the best fit *and* a consistent value for the $|\overline{\delta P}|$ within a same multiplet. A visual comparison between observed and computed spectra is shown in Figs. 7 to 10.

4.3. Discussion

Although there is no objective way of assessing the quality of a match between computed and observed periods, we adopt the following subjective one, based on the value of $|\overline{\delta P/P}|$. We consider the fitting as:

- excellent if $|\overline{\delta P/P}| \leq 0.5\%$;
- good if $0.5\% < |\overline{\delta P/P}| \leq 1.0\%$;
- satisfactory if $1.0\% < |\overline{\delta P/P}| \leq 1.5\%$;
- poor if $1.5\% < |\overline{\delta P/P}|$.

The last case (poor adjustment) may also mean that none of the periods computed from the best fitting model can account for the observed mode. According to the above criteria, we rate the quality of the matching of the periods observed in HL Tau 76 with those computed from our best fitting model. DVK give a total of 43 frequencies observed in HL Tau 76; Table 4 lists only 37 values because some frequencies are so close that they likely represent the same mode. Table 4 shows that the matching is excellent for 17 modes, good for 13 modes, satisfactory for 3 modes and poor for 3 modes. The period at 781.0 s is not matched at all and this case is discussed below. The average value of the $|\overline{\delta P/P}|$ for all the modes listed in Table 4 is 0.7%, which is currently considered as a good global fit. Even in the last category, the worst fit is only at 1.9% for the mode at 542.4 s. The overall quality of the matching may be also evaluated by estimating the mean $\sigma = (\Sigma|\overline{\delta P}|)/n$ and the root mean square $\sigma_{\rm rms} = \sqrt{(\Sigma|\overline{\delta P}|^2)/n}$ where n stands for the total number of considered modes. Here $n = 36$ since the mode at 781.0 s is not considered as a true pulsation in our analysis, as discussed below.

So, $\sigma = 4.35$ s and $\sigma_{\rm rms} = 5.27$ s. Considering that σ and $\sigma_{\rm rms}$ are calculated over a large number of modes ($n = 36$), these values confirm that the global fit is good.

We emphasize the fact that the calculated periods in Table 4 rely on the theoretical values computed for the $\ell = 1$ and $\ell = 2$, $m = 0$ modes in the best fitting model to which was applied a uniform rotational splitting as derived from the observations (DVK). However, the value for the rotational splitting has been obtained from a small number of well identified multiplets. If the observational data did not reveal any potential variation of the rotational splitting with the period, one could not exclude this variation. The assumption of a constant rotational splitting in the whole range of periods observed in HL Tau 76 contributes to the σ and $\sigma_{\rm rms}$ estimates. If part of the mismatch between observed and calculated periods is due to the assumption of a constant rotational splitting, one should find a correlation between the $|\overline{\delta P/P}|$ and the period since we expect a smooth dependence of the rotational splitting on the period. Examination of Table 4 shows a trend for the long periods to be better fit, on average, than the short periods. That may be an indication that a possible variation of the rotational splitting with period contributes to the mismatch.

The mismatch could also be partly due to the effect of a weak magnetic field. DVK suspect that such a weak magnetic field of order $1–2 \times 10^3$ G might be responsible for the asymmetry observed in the triplets of HL Tau76. However, the frequency shift induced by a weak magnetic field is predicted to increase with the g-mode order k for a given degree ℓ, i.e. increase with period (Jones et al. 1989). This is opposite to the trend in Table 4. As both a non-uniform rotational splitting and a weak magnetic field may contribute to the period mismatch, it is not possible to disantangle their effects.

The global quality of the matching shows that the selected best fitting model is well constrained and satisfactorily represents the internal structure of HL Tau 76. However, considering that HL Tau 76 has an effective temperature close to the red edge of the instability strip where the convection is supposed to increasingly interact with the pulsations, the global fit is even surprisingly good. Since the instability of the g-modes in the cool ZZ Ceti stars is mainly driven by convection (Brickhill 1990, 1991; Goldreich & Wu 1999a,b; Wu & Goldreich 1999, 2001), one would expect the largest amplitude modes to reveal the signature of the interaction with convection better than the small amplitude ones. For instance, one could speculate that as a result of the nonlinear interaction with convection the frequencies of the large amplitude modes might deviate from the

Table 4. Proposed identification of the modes.

Computed period	ℓ degree	k order	m number	Observed period(s)	$\lvert\overline{\delta P}\rvert$	$\lvert\overline{\delta P/P}\rvert$ (%)
388.5 s	2	10	2	382.5 s	6.0 s	1.5
391.1 s	2	10	–2	394.3 s	3.2 s	0.8
445.8 s	2	12	–2	449.8 s	4.0 s	0.9
497.9 s	2	14	2	493.2 s	4.7 s	0.9
498.9 s	2	14	1	494.2 s	4.7 s	0.9
500.0 s	2	14	0	495.0 s	5.0 s	1.0
550.0 s	2	16	2	540.9–541.0 s	9.0 s	1.6
551.3 s	2	16	1	541.8 s	9.5 s	1.7
552.6 s	2	16	0	542.4 s	10.2 s	1.8
590.6 s	2	17	–1	596.8–597.0–597.1 s	6.4 s	1.1
592.1 s	2	17	–2	598.6 s	6.5 s	1.1
627.1 s	2	18	–2	628.0 s	0.9 s	0.1
650.7 s	1	10	1	657.4 s	6.7 s	1.0
651.8 s	1	10	0	659.5–660.1 s	8.0 s	1.2
652.9 s	1	10	–1	661.4–661.9 s	8.8 s	1.3
667.6 s	2	20	2	662.3–662.8 s	5.1 s	0.8
669.6 s	2	20	1	663.6–664.2–665.0 s	5.3 s	0.8
692.8 s	2	21	2	689.3 s	3.5 s	0.5
741.1 s	1	12	1	738.7 s	2.4 s	0.3
743.9 s	1	12	–1	748.5 s	4.6 s	0.6
?	?	?	?	781.0 s	?	-
793.3 s	2	24	2	792.7–794.1 s	0.1 s	0.0
796.0 s	2	24	1	796.4–796.5 s	0.5 s	0.1
798.7 s	2	24	0	798.3–799.1 s	0.0 s	0.0
929.9 s	2	29	0	930.6 s	0.7 s	0.1
933.6 s	2	29	–1	932.5–933.2 s	0.8 s	0.1
964.1 s	2	30	–1	971.6 s	7.5 s	0.8
968.1 s	2	30	–2	974.4–976.4 s	7.3 s	0.7
983.5 s	2	31	2	979.2 s	4.3 s	0.4
1056.7 s	2	33	–1	1060.2 s	3.5 s	0.3
1061.4 s	2	33	–2	1061.8 s	0.4 s	0.0
1059.2 s	1	18	0	1065.0 s	5.8 s	0.5
1062.01 s	1	18	–1	1067.5 s	5.5 s	0.5
1076.4 s	2	34	2	1070.8 s	5.6 s	0.5
1308.3 s	1	23	1	1308.7 s	0.4 s	0.0
1350.6 s	2	43	–1	1347.9–1353.7 s	0.2 s	0.0
1391.2 s	2	45	0	1390.8 s	0.4 s	0.0

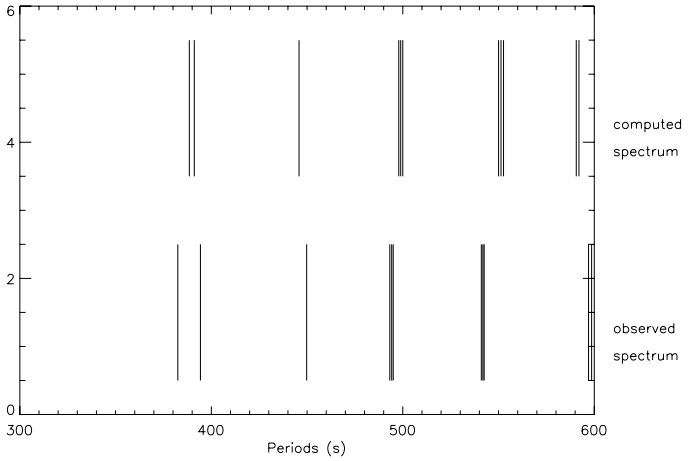

Fig. 7. Computed vs. observed spectra between 300 s and 600 s.

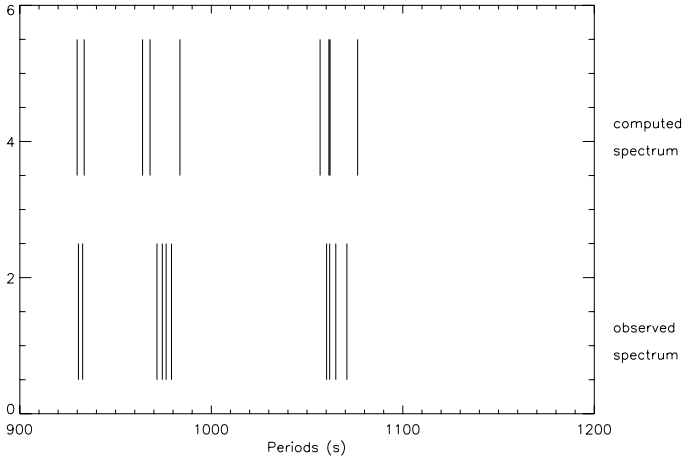

Fig. 8. Computed vs. observed spectra between 900 s and 1200 s.

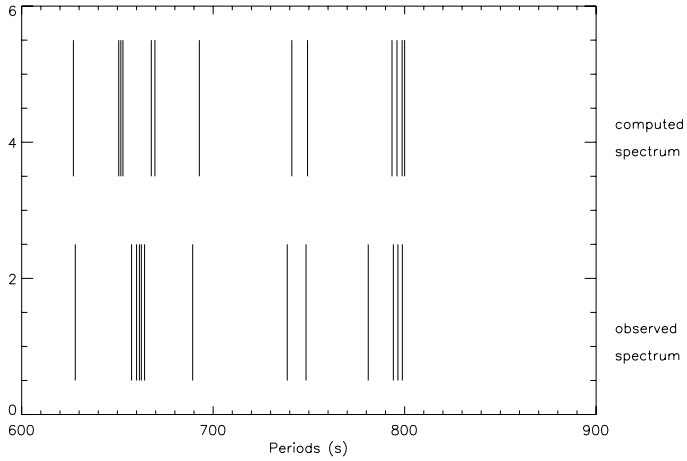

Fig. 9. Computed vs. observed spectra between 600 s and 900 s.

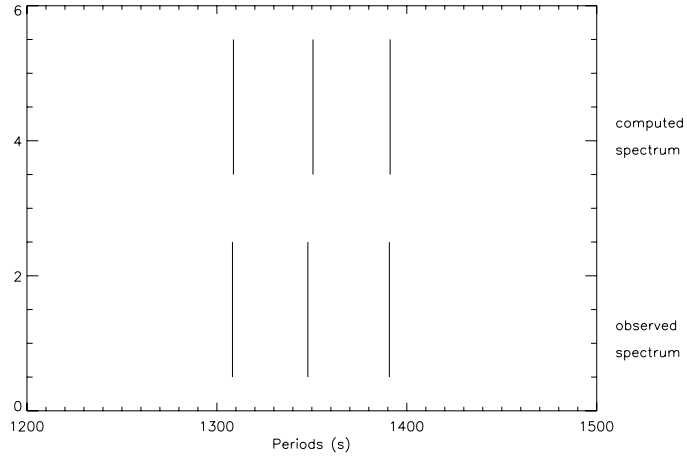

Fig. 10. Computed vs. observed spectra between 1200 s and 1500 s.

frequencies determined from the linear adiabatic calculations more than the frequencies of the small amplitude modes. By looking at the values of $|\overline{\delta P/P}|$ as a function of the mode amplitude, we find a hint of such a trend: the fit is better for the low amplitude modes than for the large amplitude ones. For the modes with an amplitude $A \leq 12$ mma, the $|\overline{\delta P/P}|$ slightly rises with increasing amplitude with a large dispersion. However, for the 4 largest amplitude modes, with periods 382.5 s, 494.2 s, 541.0 s and 597.0 s, for which $A \geq 14$ mma, the quality of the fit is never better than ≈1%. For the members of the multiplet at 541.0 s, which are the dominant modes during the two WET campaigns XCOV13 and XCOV18 (DVK), Table 4 shows that the $|\overline{\delta P/P}|$ is largest. Such a variation of the matching quality with the amplitude of the modes could reveal how the pulsation spectrum of the g-modes driven by convection in the cool ZZ Ceti stars departs from the one predicted by linear pulsation theory.

One of the predictions of the convection-driving mechanism is that the convection zone acts as a low-pass frequency filter (Goldreich & Wu 1999a). Consequently, the ratio of the amplitudes of the oscillations at the photosphere and at the bottom of the convection zone is predicted to regularly decrease with increasing frequency for a given model. In HL Tau 76, power is observed over a large range of periods, from ≈380 s to ≈1400 s but with many gaps in the power spectrum where modes are missing. It is not clear if the modes are intrinsically missing or were not detected because their amplitudes were below the detection limit at the period of the observations. Nevertheless, DVK have gathered data over a long time scale including archival data. In spite of the fact that many of the modes in HL Tau 76 are variable in amplitude, there still remain domains in the power spectrum where the modes expected from the linear nonradial computations do not appear. This is more consistent with a description of the power spectrum in terms of a series of groups of unstable modes separated by regions of stable modes than with a continuous distribution of unstable modes. We looked for a possible selection mechanism that would favourably select the modes $\ell = 1$ and $\ell = 2$ that overlap in periods. We found that among the largest amplitude modes the dominant one at 541 s is close to the overlapping modes $\ell = 1$, $k = 8$ at 557.0 s and $\ell = 2$, $k = 16$ at 552.6 s; the second largest amplitude mode at 494 s is near the overlapping modes $\ell = 1$, $k = 7$ at 499.0 s and $\ell = 2$, $k = 14$ at 500.0 s and the mode at 659.5 s to the overlapping modes $\ell = 1$, $k = 10$ at 651.8 s and $\ell = 2$, $k = 19$ at 648.2 s. The other large amplitude modes do not coincide with overlapping modes. We conclude that there is no clear evidence that the overlapping $\ell = 1$ and $\ell = 2$ modes are favourably selected.

According to the previous discussion, we identified at least three possible explanations for the slight mismatch between observed and calculated periods: the first is related to the assumption of constant rotational splitting, the second to the effect of a weak magnetic field and the third to the nonlinear effects induced by the interaction with convection. All three probably contribute to the difference between the observed periods and the periods calculated from linear pulsation theory. One of the consequences of the mismatch between observed and computed periods is that the identification of the ℓ value for the large amplitude modes may be uncertain: the frequency of a displaced large amplitude mode of degree $\ell = 1$ could be closer to the frequency of a mode $\ell = 2$ than to the frequency of a mode $\ell = 1$ as estimated from linear theory. Under theses circumstances, one cannot exclude that some of the large amplitude modes identified as $\ell = 2$ modes in Table 4 are in fact $\ell = 1$ modes whose frequencies are affected by a strong interaction with convection.

The periods at 1065 s and at 781 s were found by DVK as corresponding to linear combinations coinciding with a period predicted in the asymptotic regime. As a result, they suggested that they could be real modes. While they could not distinguish between $\ell = 1$ or $\ell = 2$ for the 1065 s period, they identified the 781 s period with a $\ell = 1$ mode. Our current results may be used to settle the ambiguous status of these two periods. We identify the 1065 s period as the mode $\ell = 1$, $k = 18$ and $m = 0$ for which our model predicts this mode at 1059.2 s. It could have been identified as the $m = -1$ in the same triplet, too, which would have given a better match. However, the high amplitude peak (9.7 mma during XCOV18) at 1067.5 s, which we identify as this $m = -1$ component, would remain unidentified in that case. We also emphasize that, with our proposed identification, the two components of this triplet have the same $|\overline{\delta P}|$ (5.8 s and 5.5 s respectively). We conclude that the period 1065 s should correspond to a real mode and is an example of mode resonance as suggested by DVK.

The case of the 781 s period is different. The closest $\ell = 1$ modes in our best fitting model are situated at 742.5 s and 801.6 s, 38.5 s and 20.6 s away from the observed period, while the closest $\ell = 2$ modes are at 759.1 s and 798.7 s, i.e. 21.9 s and 17.7 s away. Even by taking into account the rotational splitting, it is not possible to account for the 781 s by any component of these modes. We conclude that, in contrast to the 1065 s period, the 781 s pulsation is a linear combination and not a true mode.

The identifications proposed in Table 4 may be compared to the preliminary identifications by DVK for the degree of the modes. For the 36 modes listed in Table 4 we find that the identification of their ℓ degree agrees with ours for 16 modes, disagrees for 15 modes and that the identification proposed here lifts the ambiguous determination of ℓ in DVK for 5 modes. The fact that so many ℓ identifications disagree with the ones proposed in DVK is not surprising since we rely here on full calculations of the g-modes in realistic models while the preliminary identifications of DVK were based on a comparison of the observed periods with a period distribution following a constant period spacing. Kotak et al. (2002) obtained time dependent spectroscopy of HL Tau 76 from which they derived a number of frequencies in the velocity space. From the work of van Kerkwijk et al. (2000), they estimated the index R_v which measures the ratio of the amplitude in the power spectrum of the velocities and of the flux. This index is sensitive to the ℓ degree because the velocities and the flux are differently affected by the geometrical average for different values of ℓ. The time dependent spectroscopic data analysed by Kotak et al. (2002) are short and cannot resolve the numerous close frequencies of HL Tau 76. The best derived R_v for the 541 s period is a 3σ confidence level determination. For the 5 remaining periods, the R_v index is measured with a lower confidence level. From the value of this index, Kotak et al. (2002) concluded that the 6 modes they detect in HL Tau 76 are compatible with a $\ell = 1$ degree. Provided that the mode at 781 s is excluded (since we argue it is a linear combination and not a true mode), our proposed identification disagrees for 4 out of the 5 remaining modes (for periods 382.5 s, 494.2 s, 541.0 s and 597.0 s) which we find as $\ell = 2$ modes. Our identification for the pulsation with a period of 659.5 s as a $\ell = 1$ mode agrees. However, as outlined above, the periods of these modes that have the largest amplitudes may be affected by the interaction with convection and may slightly differ from the periods calculated following the linear theory as presented in the present work.

5. Conclusion

This paper has shown that it is possible to obtain tight constraints on the internal structure of the cool ZZ Ceti star HL Tau 76 by comparing the periods of g-modes from realistic models with the observed periods. Since HL Tau 76 exhibits about 40 independent modes of pulsation, it offers a unique opportunity to constrain the model and derive some of the main stellar parameters. We have computed a grid of DA white dwarf models representative of HL Tau 76 whose atmospheric parameters ($\log g$ and $T_{\rm eff}$) are well constrained by spectroscopy. We computed the periods of the $\ell = 1$ and $\ell = 2$ nonradial g-modes in the models to be compared with the observations and used a χ^2 minimum algorithm to select the model that best fits the observations. Following this approach, we determined the total stellar mass $M_\star = 0.575\ (\pm 0.005)\ M_\odot$, the hydrogen mass fraction $M({\rm H}) = 2.35 \times 10^{-4}\, M_\star$, from which we derived the helium mass fraction $M({\rm He}) = 10^{-2} M_\star$. Our method based on χ^2 is not sensitive to the effective temperature in the range of $T_{\rm eff}$ deduced from spectroscopy for HL Tau 76. Nevertheless we find that the best fit is obtained with $T_{\rm eff} = 11\,375$ K. Adiabatic calculations were carried out for the $\ell = 1$ and $\ell = 2$ pulsation modes for the best fitting candidate that delivers the periods for their $m = 0$ component. We used the *rotational splitting* determined from observations (DVK) to estimate the periods of the components of the multiplets for the $\ell = 1$ and the $\ell = 2$ modes. We were then able to match almost all the observed peaks in the power spectrum of HL Tau 76 in terms of $\ell = 1$ and $\ell = 2$ modes split by rotation and find their order k and azimuthal number m. The fitting process was satisfactory since we were capable of fitting 36 modes with an average precision of 0.7%. We found that the quality of the matching for individual modes seems to vary with the period and with the amplitude. The decreasing quality of the fit with decreasing period could be due

to the fact that the rotational splitting is not uniform in the star, while we used a constant rotational splitting to calculate the periods. A weak magnetic field would induce a period mismatch increasing with period, in the opposite way to the one deduced from our fit. The decreasing quality of the fit with increasing amplitude might be a signature of a nonlinear interaction between the convection and the pulsations. The identification of the large amplitude modes in terms of their ℓ value may be affected by this effect since we find many cases of overlapping periods for $\ell = 1$ and $\ell = 2$ modes. As a consequence, an $\ell = 1$ mode, slightly shifted in frequency because of its interaction with convection, could be located closer to the period of an $\ell = 2$ mode predicted by our linear adiabatic calculations and be misleadingly identified as a $\ell = 2$ mode. The determination of the total mass and the estimate of the hydrogen mass fraction in DA white dwarfs are important issues because of the consequences of these parameters for the age determination of the white dwarfs on the cooling sequence and the potential use of the white dwarfs for cosmochronology, distance determination to globular clusters and so on. The asteroseismological study of HL Tau 76 presented in this paper gives reliable values for these two parameters. It also provides some hints to the impact of the convection driving mechanism on the pulsation period spectrum, which deserves more theoretical work.

References

Bergeron, P., Fontaine, G., Brassard, P., et al. 1993, AJ, 106, 1987
Bergeron, P., Wesemael, F., Lamontagne, R., et al. 1995, ApJ, 449, 258
Bergeron, P., Fontaine, G., Billères, M., Boudreault, S., & Green, E. M. 2004, ApJ, 600, 404
Bradley, P. A. 1998, ApJS, 116, 307
Bradley, P. A. 2001, ApJ, 552, 326
Brassard, P., & Fontaine, G. 2005, ApJ, 622, 572
Brassard, P., Fontaine, G., Wesemael, F., Kawaler, S. D., & Tassoul, M. 1991, ApJ, 367, 601
Brassard, P., Fontaine, G., Wesemael, F., & Tassoul, M. 1992, ApJS, 81, 747
Brickhill, A. J. 1990, MNRAS, 246, 510
Brickhill, A. J. 1991, MNRAS, 251, 673
Castanheira, B. G., Kepler, S. O., Moskalik, P., et al. 2004, A&A, 413, 623
Córsico, A. H., Althaus, L. G., Benvenuto, O. G., & Serenelli, A. M. 2001, A&A, 380, L17
Córsico, A. H., Althaus, L. G., Benvenuto, O. G., & Serenelli, A. M. 2002, A&A, 387, 531
Córsico, A. H., Althaus, L. G., Montgomery, M. H., et al. 2005, A&A, 429, 277
Dolez, N., Vauclair, G., Kleinman, S. J., et al. 2006, A&A, 446, 237 (DVK)
Fleming, T. A., Liebert, J., & Green, R. F., 1986, ApJ, 308, 176
Fontaine, G., & Wesemael, F. 1997, in White dwarfs, ed. J. Isern, M. Hernanz & E. Garcia-Berro, 173
Fontaine, G., & Brassard, P. 2004, 14th European Workshop on White Dwarfs, ed. D. Koester & S. Moehler, in press
Fontaine, G., Graboske, H. C. Jr., & van Horn, H. M. 1977, ApJS, 35, 293
Fontaine, G., Brassard, P., & Bergeron, P. 2001, PASP, 113, 409
Goldreich, P., & Wu, Y. 1999a, ApJ, 511, 904
Goldreich, P., & Wu, Y. 1999b, ApJ, 523, 805
Iglesias, C. A., & Rogers, F. J. 1996, ApJ, 454, 943
Itoh, N., Kohyama, S., Matsumoto, N. & Seki, M. 1984, ApJ, 285, 758
Itoh, N., Mitake, S., Iyetomi, H., & Ichimaru, S. 1983, ApJ, 273, 774
Jones, P. W.,Hansen, C.J., Pesmell, W. D., & Kawaler, S. D. 1989, ApJ, 336, 403
Kanaan, A., Nitta, A., Winget, D. E., et al. 2005, A&A, 432, 219
Kepler, S.O., Giovannini, O., Wood, M. A., et al. 1995, ApJ, 447, 874
Kepler, S. O. Mukadam, A., Winget, D. E., et al. 2000, ApJ, 534, 185
Kleinman, S. J., Nather, R. E., Winget, D. E., et al. 1998, ApJ, 495, 424
Kleinman, S. J., Harris, H. C., Eisentein, D. J., et al. 2004, ApJ, 607, 426
Kotak, R., van Kerkwijk, M. H., Clemens, J. C., & Bida, T. A. 2002, A&A, 391, 1005
Landolt, A.U. 1968, ApJ, 153, 151
Ledoux, P., & Walraven, T. 1958, Handbuch der Physik, ed. S. Flüge (Berlin: Springer-Verlag), 51, 353
Metcalfe, T. S., Montgomery, M. H., & Winget, D. E. 2003, MNRAS, 344, L88
Metcalfe, T. S., Montgomery, M. H., & Kanaan, A. 2004, ApJ, 605, L133
Mitake, S., Ichimaru, S., & Itoh, N. 1984, ApJ, 277, 375
Montgomery, M. H., Metcalfe, T. S., & Winget, D.E. 2003, MNRAS, 344, 657
Mukadam, A. S., Kepler, S. O., Winget, D. E., et al. 2003, ApJ, 594, 961
Mukadam, A. S., Mullaly, F., Nather, R. E., et al. 2004a, ApJ, 607, 982
Mukadam, A. S., Winget, D. E., von Hippel, T., et al. 2004b, ApJ, 612, 1052
Nather, R. E., Winget, D. E., Clemens, J. C., et al. 1990, ApJ, 361, 309
Pfeiffer, B., Vauclair, G., Dolez, N., et al. 1996, A&A, 314, 182
Salaris, M., Cassisi, S., Garcia-Berro, E., Isern, J., & Torres, S. 2001, A&A, 371, 921
Tassoul, M., Fontaine, G., & Winget, D. E. 1990, ApJS, 72, 335
van Kerkwijk, M. H., Clemens, J. C., & Wu, Y. 2000, MNRAS, 314, 209
Vauclair, G., Moskalik, P., Pfeiffer, B., et al. 2002, A&A, 381, 122
Wood, M. 1995, in White Dwarfs, ed. Koester, D., & Werner, K. (Springer), 41
Winget, D. E., Hansen, C. J., Liebert, J. W., et al. 1987, APJ, 315, 77
Winget, D. E., Nather, R. E., Clemens, J. C., et al. 1991, ApJ, 378, 326
Winget, D. E., Nather, R. E., Clemens, J. C., et al. 1994, ApJ, 430, 839
Wu, Y., & Goldreich, P. 1999, ApJ, 519,783
Wu, Y., & Goldreich, P. 2001, ApJ, 546, 469